Int. J. Multiphase Flow Vol. 15, No. 3, pp. 307–325, 1989
Printed in Great Britain

0301-9322/89 $3.00 + 0.00
Pergamon Press/Elsevier

WALL SHEAR STRESS MEASUREMENTS IN VERTICAL AIR–WATER ANNULAR TWO-PHASE FLOW

A. H. GOVAN,[1] G. F. HEWITT,[1] D. G. OWEN[2]† and G. BURNETT[3]

[1]Thermal Hydraulics Division, Harwell Laboratory, Oxfordshire OX11 0RA, England

[2]CERL, Leatherhead, Surrey KT22 7SE, England

[3]Department of Chemical Engineering, Imperial College, London, England

(*Received* 15 *September* 1988; *in revised form* 15 *November* 1988)

Abstract—Measurements of wall shear stress are reported for annular two-phase air–water flow in a vertical 23 m long, 0.0318 m dia tube (the LOTUS rig at Harwell). The shear stress was measured using a hot-film probe system calibrated using both single-phase and zero-entrainment two-phase flows. The measurements were made for both equilibrium annular flow and also for the "unidirectional deposition" region following film removal. The equilibrium measurements were analysed for both average and time-varying shear stress. The average values were in good agreement with the values calculated from pressure gradient and the fluctuating values showed characteristic peak frequencies corresponding to disturbance waves. The measurements in the unidirectional deposition region showed that commonly used assumptions for the effect of droplet deposition on shear stress grossly overpredicted the effect. Better agreement was obtained by taking account of the effect of the droplets on mixing length using the correlation of Owen & Hewitt and by accounting for the deposition effect by using an analogy with condensation.

Key Words: annular two-phase flow, vertical pipes, air–water, wall shear stress, pressure drop deposition

1. INTRODUCTION

The work described in this paper had two main objectives. The first was to obtain and analyse data for wall shear stress in fully-developed annular flow and the second was to evaluate the contribution of droplet deposition to the total wall shear stress.

The average wall shear stress (τ_0) in steady vertical upwards annular flow is related to the average pressure gradient (dp/dz) by the relationship

$$-\frac{dp}{dz} = \frac{4\tau_0}{d_0} + \frac{d(MF)}{dz} + g[\epsilon_G \rho_G + (1-\epsilon_G)\rho_L], \quad [1]$$

where ϵ_G is the void fraction, g is the acceleration due to gravity, ρ_G and ρ_L are the gas and liquid densities and MF is the momentum flux, which is approximated by the expression

$$MF = \dot{m}[xu_G + E(1-x)u_d + (1-E)(1-x)u_f], \quad [2]$$

where $\dot{m}$ is the total mass flux, x is the quality, E is the fraction of the liquid phase entrained as droplets and u_G, u_d and u_f are the gas, droplet and film liquid velocities, respectively. Often the second, and sometimes the third, terms on the r.h.s. of [1] are small compared to the first term and hence the wall shear stress term is dominant in determining the pressure gradient.

Measurement of pressure gradient is arguably the most common measurement made in two-phase flow. However, direct measurements of shear stress are more difficult and therefore more rare. Of course, measurements of time-averaged wall shear stress in annular flow can be compared with values calculated from the average pressure gradients using [1]. Though it is useful to check the consistency of the two measurements via this route, the most interesting feature of local measurements of shear stress in fully-developed flow lies in their time-varying nature. In earlier work at Harwell, Martin (1983) showed how shear stress fluctuations were related to film thickness variations corresponding to the passage of large disturbance waves over the interface. Martin used the hot-film technique for measuring instantaneous local shear stress and the technique was further

†Previously at Harwell Laboratory.

developed by Whalley & McQuillan (1985). In the present experiments, probes of the type used by Whalley & McQuillan were used. The main new features of the present experiments were as follows:

(a) They were carried out for fully-developed annular flow. The measurements were made on the Harwell LOTUS rig with the measurement location being around 600 tube dia from the liquid injection point.
(b) The range of flow conditions covered was much greater with liquid mass fluxes up to 500 kg/m^2 s and gas mass fluxes up to 240 kg/m^2 s.

The data were analysed to obtain both time-averaged shear stress values and also the power spectral density curves for the fluctuations.

The second main objective of the present work was to evaluate the contribution of droplet deposition to the interfacial shear stress (τ_i) in annular flow. If, as is usually the case, the acceleration of the liquid film can be neglected, τ_i is related to τ_0 by the expression

$$\tau_0 = \tau_i\left(\frac{R_i}{R_0}\right) + \frac{1}{2}\left(\rho_L g + \frac{dp}{dz}\right)\left(\frac{R_i^2 - R_0^2}{R_0}\right), \quad [3]$$

where R_0 is the tube radius and R_i is the radial position of the interface. Often, the liquid film is rather thin and $\tau_0 \approx \tau_i$. In a fully-developed annular flow, the interfacial shear stress is enhanced (relative to the corresponding single-phase gas flow) by two mechanisms:

(1) The interface is covered by a complex pattern of waves which (as is demonstrated directly by the instantaneous wall shear stress measurements) enhance the interfacial shear in a manner analogous to that of roughness in a single-phase pipe flow.
(2) There is a continuous process of droplet deposition on the film surface and droplet entrainment from the tips of the "disturbance waves" which pass along the film. Since the depositing droplets have a higher velocity than the entraining ones, this process results in a net momentum transfer to the film, thus enhancing the shear stress.

The difficulty in trying to evaluate the relative roles of these processes is that they occur simultaneously and an increase in the effect of one usually occurs concurrently with an increase in the effect of the other. In the present experiment, an attempt has been made to "de-couple" the effects by the following means: a fully-developed annular flow was set up (using a very long vertical test section) and the liquid film was removed. Droplet deposition continues and a new film builds up; initially, until the critical film flow rate for disturbance waves is reached, there is no re-entrainment and the deposition is *unidirectional*. If the wall shear stress is measured in the unidirection deposition region, where the film is thin and the effect of interfacial roughness is relatively small, then one has a possible means of isolating the effects of the droplets *per se* on the interfacial shear. As we shall see, these effects are complex and involve not only momentum deposition on the film, but also the effects of the droplets on the gas core turbulence. As an aid to evaluating the deposition effects, measurements were made of the rate of deposition in the unidirectional deposition region; this was done by simply removing the newly deposited liquid film at various distances downstream from the initial film extraction point. Pressure drop measurements were also made, both in fully-developed flow and in the unidirectional deposition region.

2. EXPERIMENTAL TECHNIQUES AND APPARATUS

2.1. Wall shear stress measurement

A variety of techniques have been used to measure wall shear stress. Direct measurements of average wall shear stress, by measuring the restoring force, are possible (e.g. Cravarolo *et al.* 1964;

Kirillov *et al.* 1978). However, most researchers have used indirect methods based on the analogy between momentum transfer and mass transfer (e.g. Kutateladze *et al.* 1969; Cognet *et al.* 1984; Zabaras 1985) or heat transfer (e.g. Bellhouse & Schulz 1966; Shiralkar 1970; Martin 1983; Whalley & McQuillan 1985).

For the present experiments, since local fluctuating shear stress values were required, a heat or mass transfer method was needed. Since the mass transfer methods require the use of an additive (typically ferri/ferro cyanide mixture), the heat transfer method was preferred.

The shear stress probes used were similar to those used by Whalley & McQuillan (1985) and consisted of a thin film of nickel deposited onto a flexible polyamide substrate, and covered with a further thin polyamide layer to protect the probes from electrolytic attack. The layout of the probes is shown in figure 1. The substrate contains five probes but only one is used at any given time, while one of the others may be used to provide temperature compensation if required. Because the films have a lifetime of only a few weeks' use, the other probes on the substrate are wired up as spares. The connecting wires reach the solder joints through the substrate to minimize flow disturbance. The substrate is glued to the face of a Perspex plug, machined to the same diameter as the test section. By using metal shims the plug may be accurately positioned to ensure that the shear stress probe lies flush with the inside wall of the test section.

The probe is maintained at constant temperature by a standard hot-film anemometry circuit. A laminar thermal boundary layer grows on the probe in the direction of flow and the instantaneous average heat transfer coefficient for the probe is proportional to the heat flux which is in turn proportional to the square of the voltage drop, V. In an ideal developing laminar boundary layer, the heat transfer coefficient is proportional to $\tau_0^{1/3}$, hence the use of the probe for measuring wall shear stress! In practice, the instantaneous wall shear stress τ_0 is related to the probe output V by

$$V^2 = a + b\tau_0^{1/3}. \qquad [4]$$

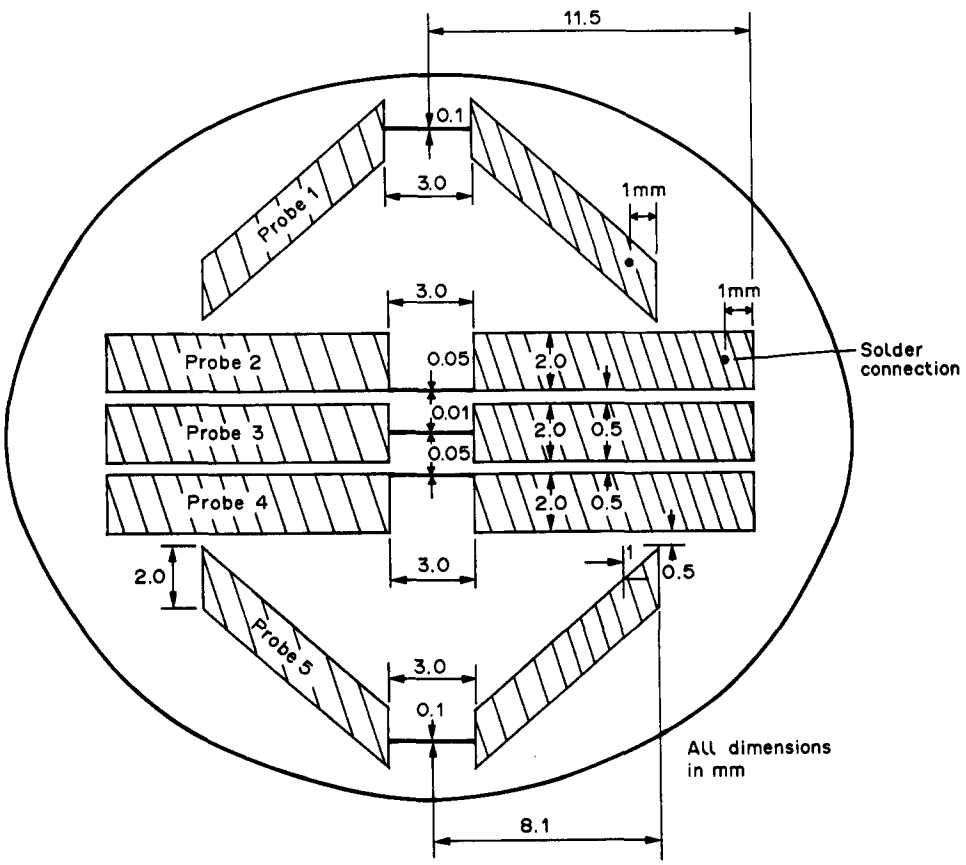

Figure 1. Layout of the hot-film probe.

The mean shear stress can be calculated from the voltage time-history in two ways. For a steady voltage, the shear stress is given by

$$\tau_0 = \left(\frac{\bar{V}^2 - a}{b}\right)^3 \quad [5]$$

but for a fluctuating voltage, as is usually obtained in two-phase flow, the average shear stress is correctly given by

$$\tau_{0AV} = \frac{\bar{V}^6 - 3a\bar{V}^4 + 3a^2\bar{V}^2 - a^3}{b^3}. \quad [6]$$

However, the use of [6] requires more sophisticated processing capabilities and in many circumstances it is more convenient to use [5]. It is shown in section 3.1.1 that this gives reasonably accurate results.

The constants a and b in [4] are conventionally obtained by calibration against known flow conditions. In the present experiments, a single-phase water flow was set up and the pressure gradient $(dp/dz)_L$ measured in the probe region using a differential pressure (DP) cell (see below). The wall shear stress is then given simply by

$$\tau_0 = \left[\left(\frac{dp}{dz}\right)_L - \rho_L g\right]\frac{d_0}{4}. \quad [7]$$

To cover the full range of shear stresses encountered in two-phase flows, large water mass fluxes (up to 8000 kg/m^2 s) were required. To achieve this it was necessary to minimize the pressure loss by injecting the water just 2.66 m (83 dia) upstream of the probe. This was inconvenient for repeated calibrations and an alternative supplementary calibration technique was developed. If the water flowrate is below that for the onset of disturbance waves, then there are no entrained droplets and, under these conditions, wall shear stress may be estimated accurately from pressure gradient using [1] and [2]. Thus, these conditions were used for the two-phase flow calibration. The three terms on the r.h.s. of [1] represent the effect of wall friction, acceleration and gravity, respectively. In the conditions used for the two-phase flow calibration, the acceleration and gravity terms are small compared to the frictional term and can be estimated with sufficient accuracy using a calculated value of ϵ_G. In the present work, ϵ_G was calculated by estimating the film thickness δ from the known film flowrate and the measured pressure gradient using the "thin film" version of the "triangular relationship" described in detail by Hewitt (1982); ϵ_G is then given by

$$\epsilon_G \approx 1 - \frac{4\delta}{d_0}. \quad [8]$$

Figure 2 shows a typical calibration using zero-entrainment annular flow. From the scatter in this graph the uncertainty in the measured value of τ was estimated to be about 5% for values of τ around 15 N/m^2, rising to about 9% for values of τ around 40 N/m^2. This takes into account the third-power dependence of τ on V^2. As will be seen below, the two-phase flow and single-phase flow calibrations gave reasonably consistent results.

The probe voltage was measured using the bridge CTA 56C16 manufactured by DANTEC. For the equilibrium measurements the anemometer 56C01 was used. This does not have temperature compensation and so it was necessary to use a temperature correction, as recommended by the manufacturers. For the shear stress measurements in a depositing film, which were carried out at a later stage, the temperature-compensating anemometer 56C14 was used instead. In both cases an integrating voltmeter was used to give the mean voltage while for the equilibrium measurements only, the time-history was recorded on magnetic tape and analysed on a minicomputer.

2.2. Pressure drop

Measurements of pressure drop are important in the interpretation of the shear stress data. Extensive pressure gradient (and also film flowrate) data had already been obtained for the conditions of the fully developed annular flow tests. These have been reported by Owen *et al.* (1985) and tabulated by Owen (1986). Confirmatory tests were carried out as part of the present

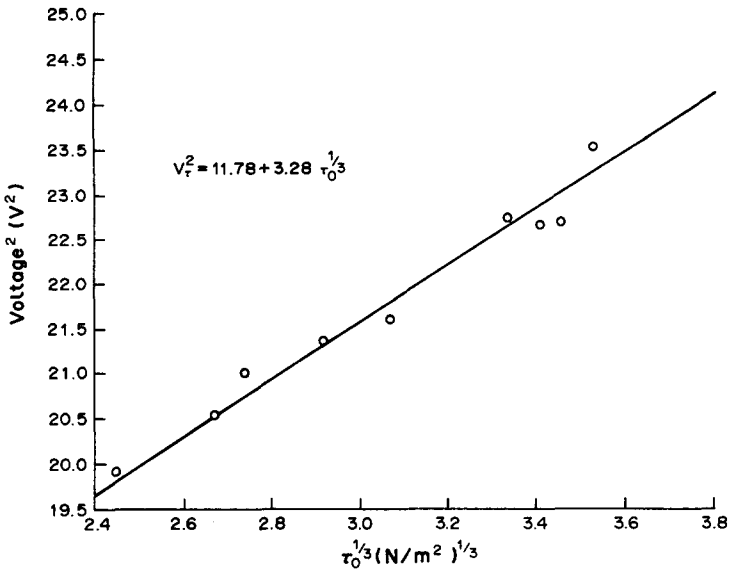

Figure 2. Typical hot-film calibration using a two-phase flow.

experiments. However, a new series of pressure drop measurements were carried out relevant to the unidirectional deposition tests. Here, the tappings were 0.275 m apart with the first tapping 0.105 m above the first film removal porous wall section (see figure 3).

The pressure tappings were connected, via water filled lines, to a Kent electronic DP cell. Care was taken to purge the lines to ensure that no air bubbles were present in them. As is always the case in two-phase flow, there were fluctuations in the pressure gradient and these were a significant fraction of the total pressure drop measured in the unidirectional deposition experiment. The output from the DP cell was passed through an amplifier with a long time constant (several seconds) to remove the higher frequency fluctuations and make it easier to read the average value. There was no possibility of increasing the length over which pressure drop was measured in these tests since it was mandatory that the measurements should be made in the (short) redeposition zone.

2.3. Deposition measurements

In the second series of experiments wall shear stress was measured in the unidirectional deposition region following the removal of the liquid film. In interpreting the results of these measurements, it was important to determine the *rate* at which droplet deposition was occurring. This could be done quite simply by removing the reformed liquid film through a second porous wall section placed at a known distance downstream. The porous wall sections are constructed from sintered metal tubes of the same internal diameter as the test section and 0.075 m long. This technique has been extensively used (e.g. Cousins & Hewitt 1968). Some gas is inevitably removed with the liquid and it is important that this is minimized, particularly at the upstream porous wall section. In the measurements described here the gas take-off at the first sinter was typically around 1% of the total gas flow. Measurements were made with deposition lengths (measured between the ends of the porous wall) of 0.16, 0.32 and 0.45 m. The experimental layout is shown in figure 3.

2.4. Apparatus and procedure

All the experiments were carried out on the LOTUS (LOng TUbe System) rig at Harwell (see Owen 1986). This consists of a 23 m long, 0.0318 m dia vertical copper pipe to which can be fed a metered supply of filtered compressed air and a metered supply of demineralized water. Air flow metering was done using a standard orifice and water flow metering by means of a set of calibrated variable area flowmeters. In the present experiments the air entered at the bottom of the tube and the water was introduced 2 m further up through a porous wall section. All the measurements were

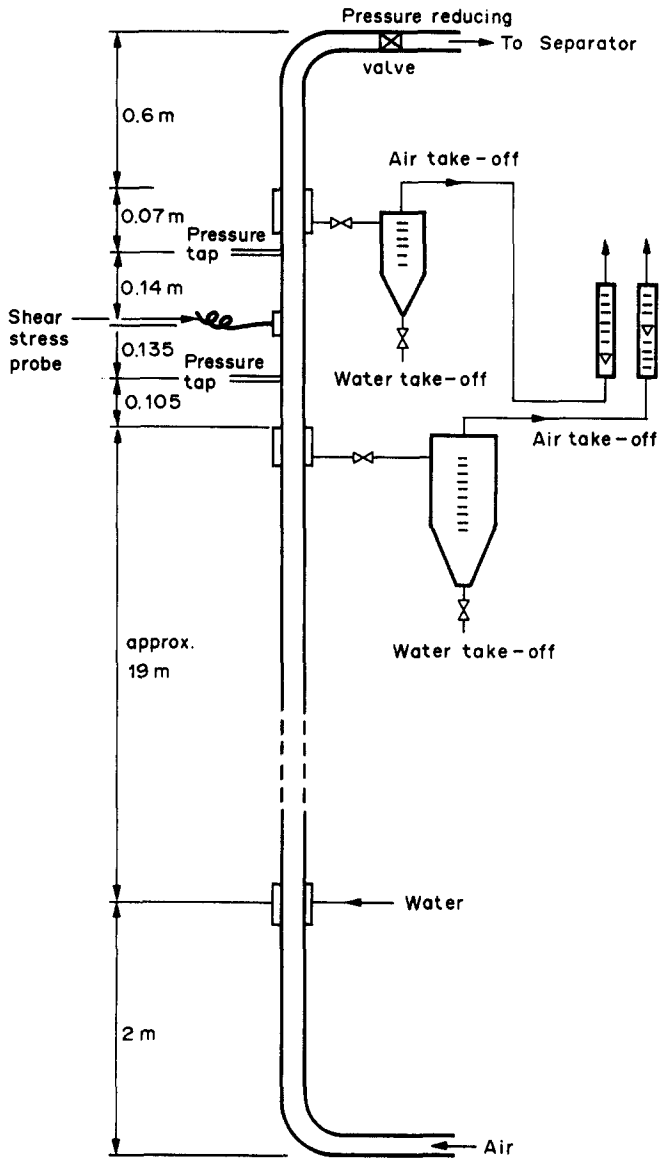

Figure 3. Experimental arrangement for deposition measurements.

taken near the top of the test section at a distance of about 600 dia from the liquid inlet, but not less than 0.6 m from the test section outlet.

For the equilibrium shear stress tests, the measurements were made at a distance of 20 m from the liquid injector with pressure tappings at 18.1 and 19.4 m. The pressure at a distance of 19 m from the injector (i.e. between the pressure tappings) was maintained at 3.63 b by throttling the outlet. Tests were carried out at liquid mass fluxes of 100, 200, 300 and 500 kg/m^2 s with gas mass flux being varied in the typical range 70–240 kg/m^2 s for each liquid flowrate. The fluid temperature in these tests was close to ambient (i.e. 20 ± 3°C).

The tube layout for the unidirectional deposition tests is shown in figure 3. In this case the experiments were carried out at a pressure of 2.40 b (measured just upstream of the first take-off sinter) with liquid mass fluxes of 100, 150 and 200 kg/m^2 s and gas mass flux values of 100, 110, 120, 130 and 140 kg/m^2 s for each of the liquid mass fluxes. In order to compare the deposition wall shear stresses with those for equivalent flows with no deposition, measurements were also made in equilibrium annular flow at the same pressure (2.4 b) and the same range of gas mass fluxes, with liquid mass fluxes of 5, 6 and 7 kg/m^2 s. These flowrates are below the value necessary for the onset of entrainment and are in the same range as the measured film flowrates in the deposition experiment.

3. RESULTS AND DISCUSSION

3.1. Fully-Developed Annular Flow

3.1.1. Mean shear stress

Table 1 gives the full list of shear stress measurements and compares the values obtained with single-phase and two-phase calibrations using each of the two equations [5] and [6]. It can be seen that [6] gives slightly higher values. The table also shows that the results using the single-phase and two-phase calibrations agree to within about 10% on average.

Using the pressure gradient and entrained liquid fraction data obtained for identical conditions by Owen *et al.* (1985) and tabulated in detail by Owen (1986), τ_0 was also calculated from the

Table 1. Shear stress measurements in equilibrium annular flow

		Wall shear stress (N/m^2)				
		Single-phase calibration		Two-phase calibration		Values based on experimental dp/dz measurements
$\dot{m}_G$ ($kg/m^2\,s$)	$\dot{m}_L$ ($kg/m^2\,s$)	τ_0	τ_{0AV}	τ_0	τ_{AV}	
74.3	99.9	6.0	7.7	8.5	9.7	12.5
82.6	99.9	10.6	12.5	12.9	14.2	15.5
93.0	99.9	12.3	14.0	14.4	15.5	18.6
102.7	99.9	18.9	20.7	20.0	21.2	21.3
111.5	99.9	18.2	19.8	19.4	20.5	23.2
120.7	99.9	19.6	21.1	20.6	21.6	25.8
130.9	99.9	20.3	21.7	21.2	22.1	26.4
140.4	99.9	24.4	25.8	24.5	25.4	27.8
149.5	99.9	24.6	25.8	24.7	25.4	29.5
158.7	99.9	32.6	34.0	31.0	31.8	31.4
172.3	99.9	30.6	31.8	29.4	30.2	34.5
183.9	99.9	36.6	37.8	34.0	34.8	37.0
198.9	99.9	35.4	36.5	33.1	33.8	40.3
208.0	99.9	37.5	38.5	34.8	35.3	42.6
82.5	200.0	15.9	17.3	17.5	18.4	20.8
90.8	200.0	24.0	25.5	24.2	25.2	23.3
116.1	200.0	23.8	25.0	24.0	24.8	29.6
129.7	200.0	26.2	27.6	26.0	26.8	31.9
144.8	200.0	27.5	28.8	27.0	27.8	34.0
159.3	200.0	29.3	30.5	28.4	29.2	35.5
175.3	200.0	36.9	38.2	34.3	35.1	37.3
193.2	200.0	35.4	36.4	33.1	33.8	40.3
210.3	200.0	41.3	42.3	37.6	38.2	44.1
224.1	200.0	44.2	45.2	39.8	40.4	47.8
242.9	200.0	50.1	51.1	44.2	44.7	53.7
99.5	399.3	35.3	37.2	33.0	34.2	33.8
109.1	399.3	36.4	37.7	33.9	34.7	37.4
123.5	399.3	42.2	43.5	38.3	39.1	41.4
138.0	399.3	52.6	54.2	46.0	46.9	43.7
152.7	399.3	45.0	46.5	40.4	41.3	44.6
171.3	399.3	45.9	47.4	41.0	41.9	44.1
184.2	399.3	45.3	46.7	40.6	41.4	43.3
197.5	399.3	52.0	53.4	45.6	46.4	43.9
215.0	399.3	53.2	54.5	46.4	47.2	46.3
231.1	399.3	58.8	60.1	50.5	51.3	50.2
104.5	499.3	35.1	36.9	32.9	34.0	39.5
114.2	499.3	34.3	36.0	32.3	33.3	42.6
127.0	499.3	39.5	40.6	36.2	36.9	46.3
139.2	499.3	54.1	55.6	47.1	48.0	48.9
155.2	499.3	50.1	51.6	44.2	45.0	50.6
169.4	499.3	46.5	47.8	41.5	42.3	50.8
180.4	499.3	45.5	46.9	40.8	41.6	50.2
194.7	499.3	48.2	49.5	42.7	43.6	49.1
212.6	499.3	54.0	55.4	47.0	47.8	49.2
228.8	499.3	54.5	55.6	50.7	51.3	51.5
60.9	20.1	12.3	14.0	14.4	15.5	20.0
61.0	40.2	16.5	18.6	18.0	19.4	18.3
61.5	81.0	15.6	17.5	17.2	18.5	16.6
80.1	20.1	12.7	13.7	14.7	15.4	19.2
80.1	40.2	11.5	12.4	13.6	14.3	20.0

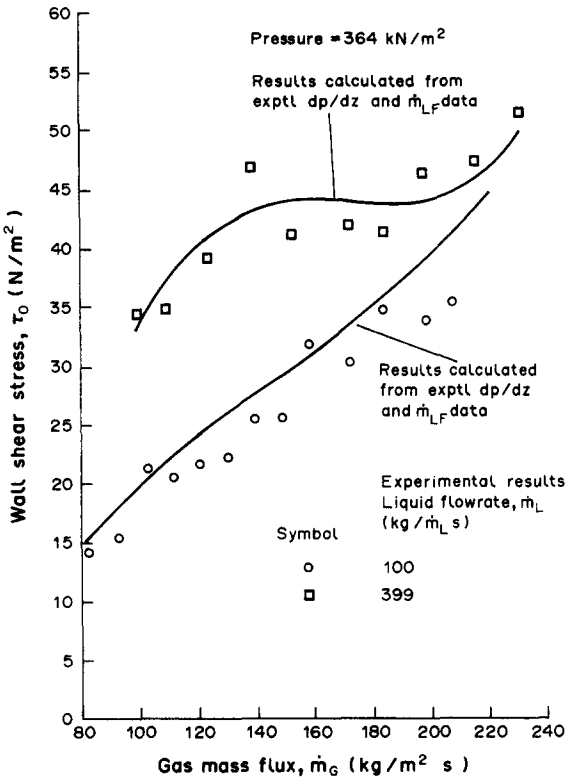

Figure 4. Comparison of experimental shear stress values and results calculated from the experimental pressure gradient and film flowrate data.

pressure gradient via [1] and [2]. Here, it was assumed that the droplet-laden gas core was a homogeneous mixture ($u_d = u_G$). The film thickness, and hence ϵ_G and u_f, were calculated assuming the universal velocity profile in the film (see Owen *et al.* 1985). Again, the second and third terms on the r.h.s. of [1] (i.e. acceleration and gravity) were small for fully developed flow, compared with the frictional (wall shear stress) term. Values calculated by this procedure are also tabulated in table 1.

The measured shear stress values are in quite good agreement with the values calculated from the pressure gradients, as is also illustrated by figure 4 which plots some of the results. At high liquid mass fluxes, the shear stress values also show a characteristic maximum and minimum as had been observed in the pressure gradient data (see Owen *et al.* 1985).

3.1.2. Time variation of shear stress

The instantaneous shear stress probe voltages, as recorded on the tape recorder, were computer processed using [4] to give records of instantaneous shear stress; examples of the time variation of τ_0 are shown in figure 5. The power spectral density of the shear stress time-history could also be obtained using a standard data processing program available on the minicomputer used. Examples of the corresponding power spectral density are also shown in figure 5. It was found that at gas mass fluxes below about 100 kg/m² s there was usually just one well-defined peak in the power spectral density, but at higher gas flowrates the power spectral density shows a multitude of smaller peaks. As was shown by Martin (1983), the peaks in instantaneous shear stress correspond to the passage of disturbance waves. Thus, the shear stress data can be used to give information on wave frequencies in annular flow. The frequency at which the maximum in the power spectral density occurs (corresponding to the peak disturbance wave frequency) increases with increasing gas flowrate, as shown in figure 6. These observations are in agreement with the results of Sekoguchi *et al.* (1985) and Azzopardi *et al.* (1979) who found that at low gas flowrates the disturbance waves are well-defined but as the gas flow is increased irregular waves appear between the dominant disturbance waves which are progressively less visible in the time-history traces. At still higher gas flows, the film flowrate is greatly reduced by droplet entrainment [as shown by Owen *et al.* (1985)] and the disturbance waves are much reduced in size.

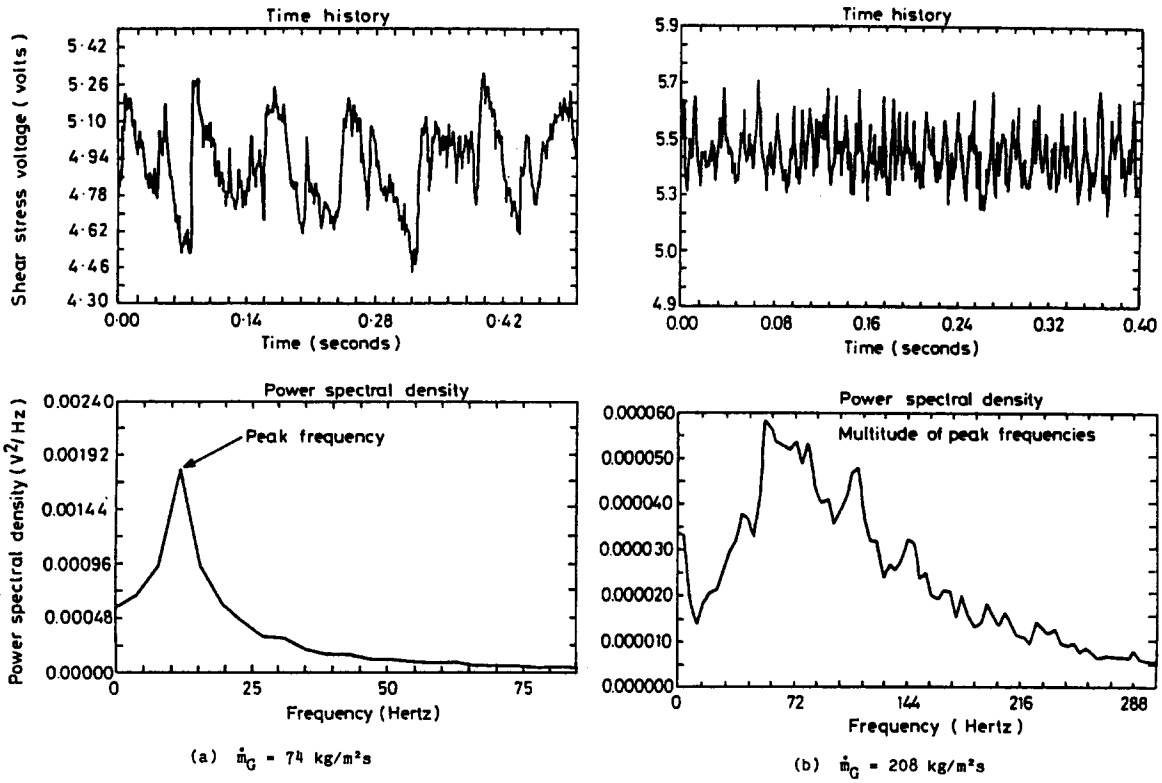

Figure 5. Shear stress fluctuations in equilibrium annular flow ($\dot{m}_L = 100\ \mathrm{kg/m^2\,s}$).

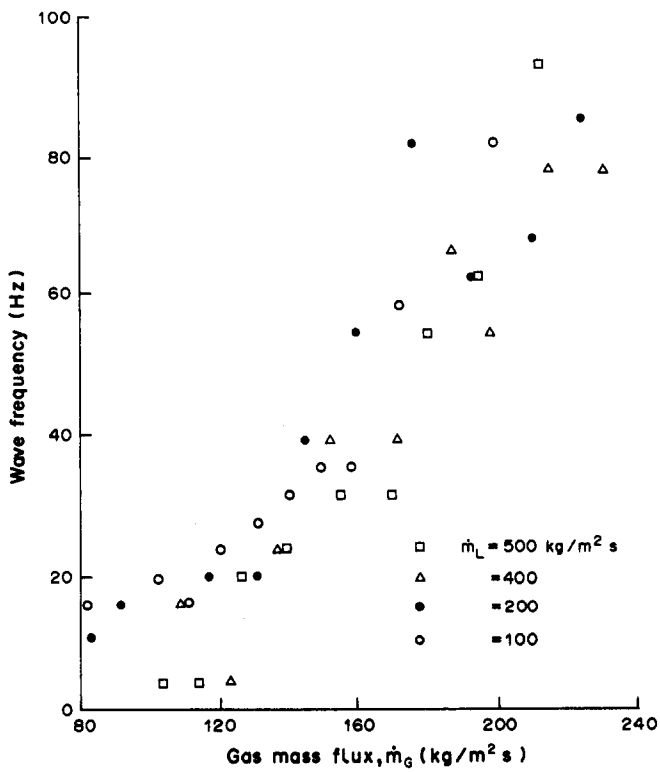

Figure 6. The variation of wave frequency with gas mass flux.

Table 2. Deposition measurements

$z_D = 0.45$ m				$z_D = 0.325$ m			$z_D = 0.16$ m		
$\dot{m}_G$ (kg/m² s)	$\dot{m}_{LF1}$ (kg/m² s)	$\dot{m}_{LF2}$ (kg/m² s)	k_D (m/s)	$\dot{m}_G$	$\dot{m}_{LF2}$	k_D	$\dot{m}_G$	$\dot{m}_{LF2}$	k_D
				$\dot{m}_L = 100 kg/m^2 s$					
				95	7.65				
100	40.1	9.85	0.110	(100)	(7.50)	0.114	(100)	(4.04)	0.124
				108	7.32		103	3.99	
110	33.9	9.55	0.105	(110)	(7.33)	0.110	(110)	(3.89)	0.118
				117	7.27		110	3.90	
120	31.0	9.50	0.109	(120)	(7.22)	0.113	(120)	(3.76)	0.119
							121	3.71	
				128	7.17	0.115	129	3.70	
130	27.7	9.25	0.109	(130)	(7.16)		(130)	(3.67)	0.120
				129	7.12	0.119	140	3.61	
140	25.3	9.13	0.111	(140)	(7.12)		(140)	(3.61)	0.123
				$\dot{m}_L = 150 kg/m^2 s$					
100	47.1	11.15	0.070	(100)	(8.97)	0.077	(100)	(4.90)	0.084
				103	8.75		102	4.78	
110	37.8	10.5	0.066	(110)	(8.36)	0.072	(110)	(4.31)	0.075
				116	8.13		111	4.28	
120	33.0	10.15	0.067	(120)	(7.81)	0.070	(120)	(4.02)	0.073
				130	7.37		122	3.97	
130	28.5	9.7	0.066	(130)	(7.40)	0.069	(130)	(3.87)	0.073
				137	7.27		130	3.91	
140	26.0	9.4	0.068	(140)	(7.19)	0.071	(140)	(3.78)	0.075
							142	3.77	
				$\dot{m}_L = 200 kg/m^2 s$					
100	55.5	12.0	0.053	(100)	(10.14)	0.062	(100)	(5.80)	0.071
				101	10.0		102	5.58	
110	43.7	11.4	0.051	(110)	(8.93)	0.055	(110)	(4.86)	0.060
				112	8.75		111	4.80	
120	33.6	10.6	0.048	(120)	(8.13)	0.051	(120)	(4.22)	0.053
				121	8.07		122	4.13	
130	29.0	(10.1)	0.048	(130)	(7.67)	0.051	(130)	(3.86)	0.051
				132	7.59		132	3.82	
140	25.8	9.55	0.049	(140)	(7.40)	0.052	(140)	(3.72)	0.052
				142	7.37		144	3.69	

Test section pressure = 2.4 b. Values in parentheses are interpolated.

3.2. Unidirectional Deposition Tests

3.2.1. Deposition rates

The data from the droplet deposition rate tests are given in table 2. This gives values of $\dot{m}_{LF1}$, the liquid film mass flux (i.e. the film flowrate per unit cross-sectional area of the tube) at the first film removal location and $\dot{m}_{LF2}$, the mass flux of the reformed film at a distance z_D from the first film removal. The mass flux ($\dot{m}_{LE}$) of the remaining liquid droplets at each location can be calculated from

$$\dot{m}_{LE1} = \dot{m}_L - m_{LF1} \quad [9]$$

and

$$\dot{m}_{LE2} = \dot{m}_L - \dot{m}_{LF2} - \dot{m}_{LF1}. \quad [10]$$

D, the droplet deposition rate per unit peripheral area of the tube is often calculated from the equation

$$D = k_D C, \quad [11]$$

where k_D is a deposition mass transfer coefficient and C is a homogeneous mean droplet concentration in the gas core calculated on the basis of homogeneous flow as follows:

$$C = \frac{\dot{m}_{LE}}{\frac{\dot{m}_G}{\rho_G} + \frac{\dot{m}_{LE}}{\rho_L}}. \quad [12]$$

For $\rho_G \ll \rho_L$ (as in the present experiments) C is given by

$$C = \frac{\dot{m}_{LE}\rho_G}{\dot{m}_G}. \quad [13]$$

Recognizing that

$$D = -\frac{\frac{\pi d_0^2}{4}}{\pi d_0} \cdot \frac{d\dot{m}_{LE}}{dz} \quad [14]$$

and integrating over the deposition length z_D we have the following expression for k_D in terms of the experimentally determined values of $\dot{m}_{LE1}$ and $\dot{m}_{LE2}$:

$$k_D = \frac{d_0}{4z_D}\frac{\dot{m}_G}{\rho_G}\ln\frac{\dot{m}_{LE1}}{\dot{m}_{LE2}}. \quad [15]$$

The variation of $\dot{m}_{LF2}$ with z_D is shown in figure 7 for the five gas flowrates used in the shear stress measurements; the specific values were obtained by interpolation, as indicated in table 2. Note that the interpolation was performed by fitting curves on a graph of $\dot{m}_{LF2}$ vs $\dot{m}_G$, therefore some smoothing has been carried out.

The values of k_D calculated from the $\dot{m}_{LF1}$ and $\dot{m}_{LF2}$ measurements are given in table 2. k_D is seen to decrease with increasing deposition length [as observed in the early work of Cousins & Hewitt (1968)] and to also decrease significantly with increasing concentration as shown, for instance, by Govan *et al.* (1988). The trends and actual numerical values are consistent with these other studies.

3.2.2. Pressure gradient

The pressure gradient data measured between distances 0.105 and 0.38 m downstream of the first film removal section are shown in figure 8. As was mentioned above, the pressure drop measurements were over rather short distances and were found to fluctuate considerably, in spite of the smoothing amplifier mentioned in section 2.2. The error bars in figure 8 indicate the magnitude of the fluctuations. Also shown in figure 8 are curves representing the pressure gradient in the absence of droplet entrainment, these values being obtained from the tables and graphs of Owen (1986). Curves for zero liquid flow, and for equilibrium annular flow with $\dot{m}_L = 5.3$ and $\dot{m}_L = 10.5$ kg/m^2 s are shown. The estimated film mass fluxes at the mid point of the zone over which the pressure gradient is measured are given as the figures within the points. Somewhat surprisingly, at first sight, it is seen that the pressure gradient is usually actually lower than the values obtained for fully-developed flow in the absence of droplet entrainment. Though, as we shall see below, the

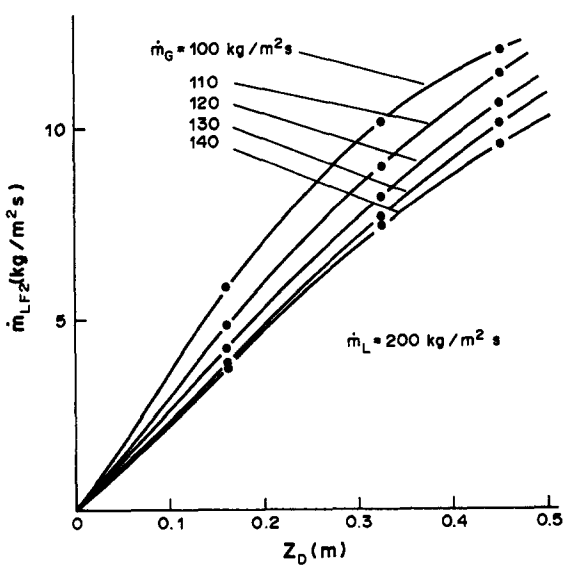

Figure 7. Deposited film flow vs distance.

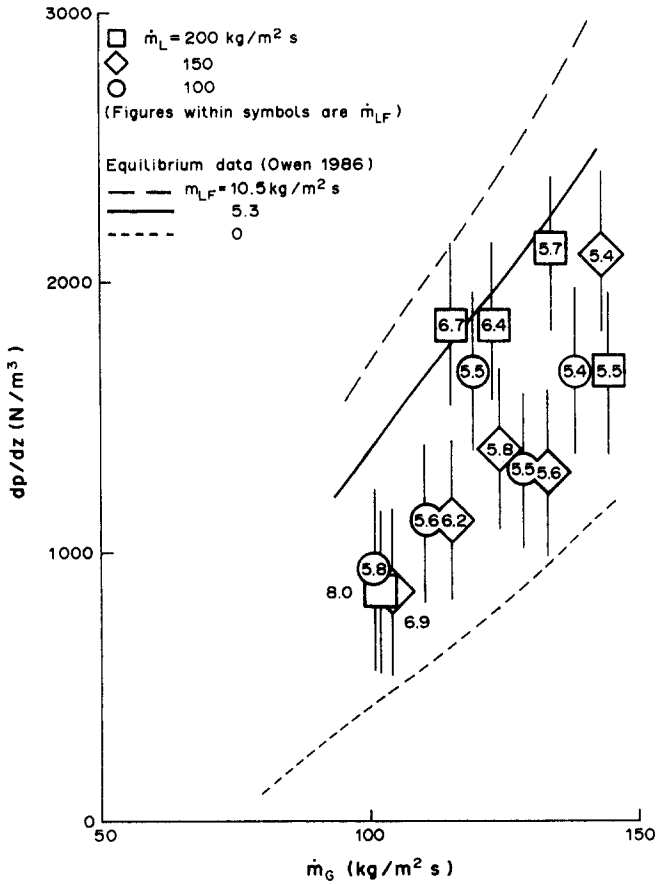

Figure 8. Pressure gradient in unidirectional deposition.

wall shear stress is enhanced in the deposition region thus tending to increase pressure gradient, this is more than offset by the pressure recovery which occurs due to the loss of gas core momentum.

The consistency of the pressure gradient and shear stress measurements can be checked, again using [1]. Ignoring the small effect of gas-phase density changes and assuming that, in the gas core, the droplets and gas travel at the same velocity and that the core liquid volume flux is small compared to the core gas volume flux, [1] reduces to

$$-\frac{dp}{dz} = \frac{4\tau_0}{d_0} + U_G \frac{d\dot{m}_{LE}}{dz} + g\rho_H(1-\epsilon_f) + g\epsilon_f\rho_L, \qquad [16]$$

where U_G is the superficial gas velocity (assumed equal to the core velocity since the film thickness is small), ϵ_f is the fraction of the cross-section occupied by the liquid film and ρ_H is the homogeneous core density, given by

$$\rho_H = \frac{\dot{m}_{LE} + \dot{m}_G}{\frac{\dot{m}_{LE}}{\rho_L} + \frac{\dot{m}_G}{\rho_G}}. \qquad [17]$$

For a thin liquid film, ϵ_f is given by

$$\epsilon_f = \frac{\pi d_0 \delta}{\frac{\pi d_0^2}{4}} = \frac{4}{d_0}\delta, \qquad [18]$$

where δ is the film thickness. From [15] we have

$$\frac{d\dot{m}_{LE}}{dz} = \frac{4D}{d_0} \qquad [19]$$

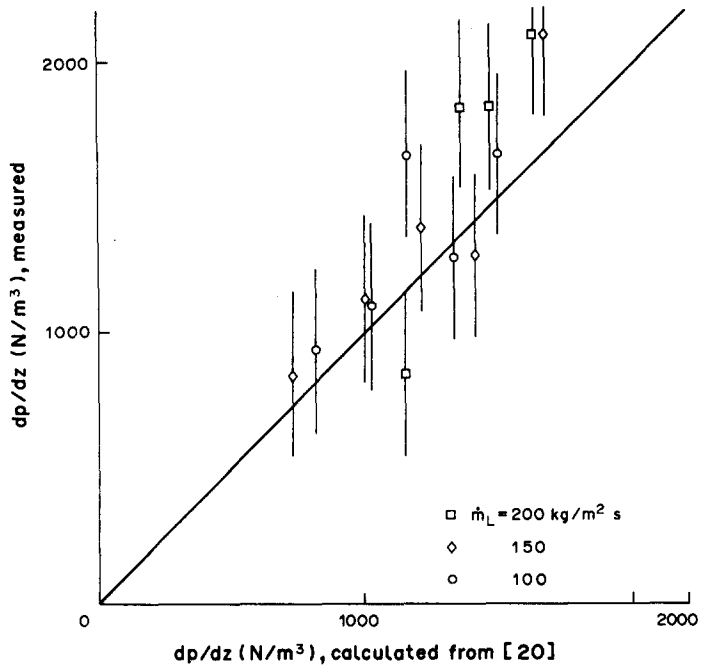

Figure 9. Comparison of measured and calculated pressure gradient in unidirectional deposition.

and, for $\rho_H \ll \rho_L$ and $\epsilon_f \ll 1$, [16] becomes

$$-\frac{dp}{dz} = \frac{4}{d_0}(\tau_0 - DU_G + \rho_L g\delta) + \rho_H g. \qquad [20]$$

Thus, dp/dz can be calculated from [20] using the measured value of τ_0 in the presence of deposition (τ_{dep}), the value of δ calculated by the thin film theory (Hewitt 1982), the value of ρ_H calculated from the known gas core droplet entrained flow and the measured value of D. Values of dp/dz calculated by this method are compared with the measured values in figure 9. Bearing in mind the scatter in the data, the agreement is seen to be rather good. The calculations showed that the dominant terms in [20] were the wall shear stress and deposition terms, the latter (giving a pressure recovery) was usually of the order of one-half of the shear stress term.

3.2.3. Wall shear stress

The prime objective in the unidirectional deposition experiment was to compare the shear stress, for the same film flow conditions, in the absence and in the presence of entrained droplets. To give a basis for comparison, measurements were made for annular flows without entrainment (i.e. in the subcritical condition with no disturbance waves). The results are shown in figure 10. These results were used to evaluate a comparative value (τ_{nodep}), at identical film flow and gas flowrates, for comparison with the τ_0 value (τ_{dep}) measured in the presence of depositing droplets. It is assumed that in the experiments with deposition the liquid film is not greatly different from the fully-developed film (measurements in condensing flows suggest that for a *smooth* film this is reasonable). It is also assumed that the wavy liquid film, which was removed 14 dia upstream, has little influence on the gas velocity profile at the shear stress probe position (since single-phase flows relax relatively quickly this seems reasonable).

The measured values of τ_{dep} and the interpolated values of τ_{nodep} are given in table 3. τ_{dep} is in the range 15–50% higher than τ_{nodep}. We shall now discuss comparisons of this data with various hypotheses on the role of droplet transfer in enhancing shear stress.

Observations of depositing droplet velocity by Cousins & Hewitt (1968) showed that it was quite close to the gas velocity and a very simple hypothesis would be that the contribution to the shear stress by the droplet deposition is simply given by

$$\tau_{drops} = DU_G = \tau_{dep} - \tau_{nodep}. \qquad [21]$$

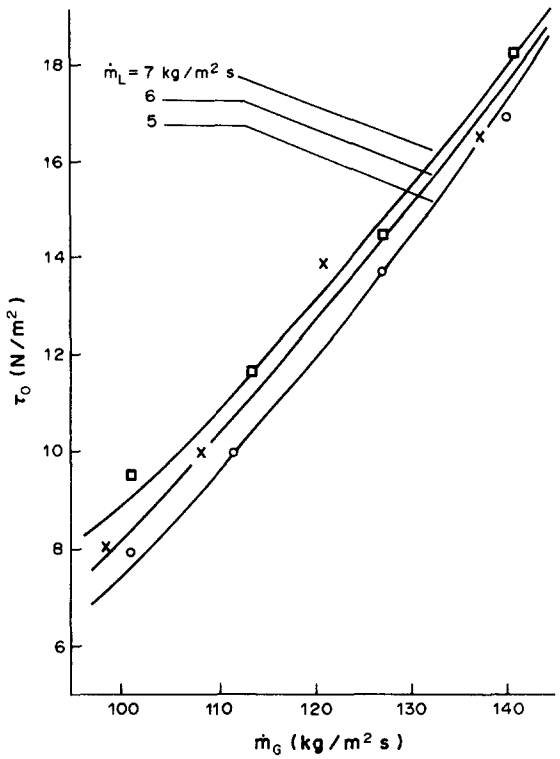

Figure 10. Shear stress in equilibrium annular flow with no entrainment.

A test of this commonly used hypothesis is shown in figure 11 and it is clear that the predicted values from [21] are much higher than the measured ones. Although the assumption that the gas and drop velocities are equal may be in error, the discrepancy should decrease as U_G is increased but this is clearly not the case. Thus, this simple analysis does not apply.

Another common approach is to consider the gas core as a homogeneous "soup", with density ρ_H, where behaviour is analogous to a multicomponent gas mixture. If the flow is in the fully-rough region, and if we assume that the volume flow of the droplets is small compared to the volume flow of the gas, then we would have

$$\frac{\tau_{dep}}{\tau_{nodep}} = \frac{\rho_H}{\rho_G}. \qquad [22]$$

Table 3. Deposition shear stress measurement

$\dot{m}_L$ (kg/m² s)	$\dot{m}_G$ (kg/m² s)	τ_{dep} (N/m²)	$\dot{m}_{LF}$ at probe (kg/m² s)	D (kg/m² s)	τ_{nodep} (N/m²)	K_{TP}	$\frac{\rho_H}{\rho_G}$	$\frac{f_i}{f_G}$	β
100	100	10.9	5.8	0.168	8.1	0.25	1.54	0.65	1.40
	110	13.6	5.65	0.167	10.2	0.25	1.55	0.65	1.34
	120	15.5	5.5	0.168	12.4	0.26	1.53	0.65	1.305
	130	17.5	5.45	0.169	14.8	0.26	1.51	0.66	1.277
	140	19.6	5.4	0.170	17.4	0.26	1.50	0.67	1.253
150	100	12.4	7.1	0.197	9.0	0.22	1.96	0.55	1.427
	110	12.6	6.4	0.196	10.7	0.22	1.97	0.55	1.391
	120	15.3	5.9	0.184	12.7	0.22	1.93	0.55	1.329
	130	17.5	5.7	0.171	15.0	0.23	1.89	0.56	1.277
	140	19.8	5.5	0.165	17.5	0.23	1.85	0.57	1.247
200	100	15.0	8.2	0.210	9.6	0.21	2.36	0.50	1.427
	110	16.2	7.0	0.197	10.9	0.21	2.35	0.50	1.384
	120	18.1	6.3	0.190	12.9	0.21	2.33	0.50	1.335
	130	19.8	5.8	0.185	15.1	0.21	2.27	0.50	1.300

Test section pressure = 2.6 b.

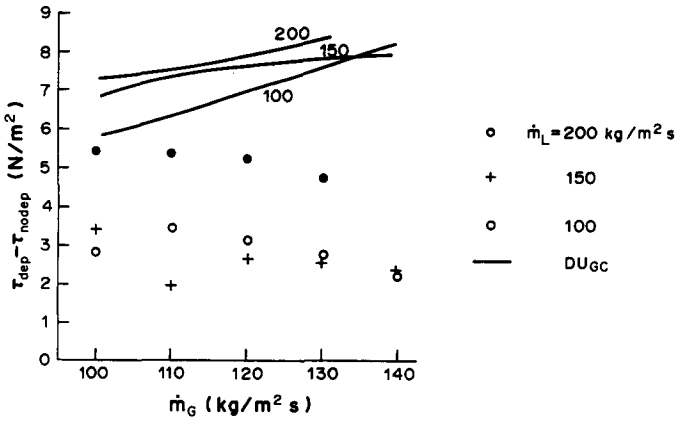

Figure 11. Contribution to shear stress from depositing droplets.

The data are compared with this equation in figure 12 and it will be seen that [22] also grossly overpredicts the enhancement of shear stress.

Another form of equation often used in annular flow is that relating the interfacial friction factor to film thickness. Examples are the equation of Wallis (1970),

$$f_{gsci} = f_{gsc}\left(1 + 360\frac{\delta}{D}\right), \qquad [23]$$

and that of Whalley & Hewitt (1978),

$$f_{gsci} = f_{gsc}\left[1 + 24\left(\frac{\rho_L}{\rho_G}\right)^{1/3}\frac{\delta}{D}\right], \qquad [24]$$

where f_{gsci} is defined as

$$f_{gsci} = \frac{\tau_i}{\frac{1}{2}\rho_H U_G^2} \qquad [25]$$

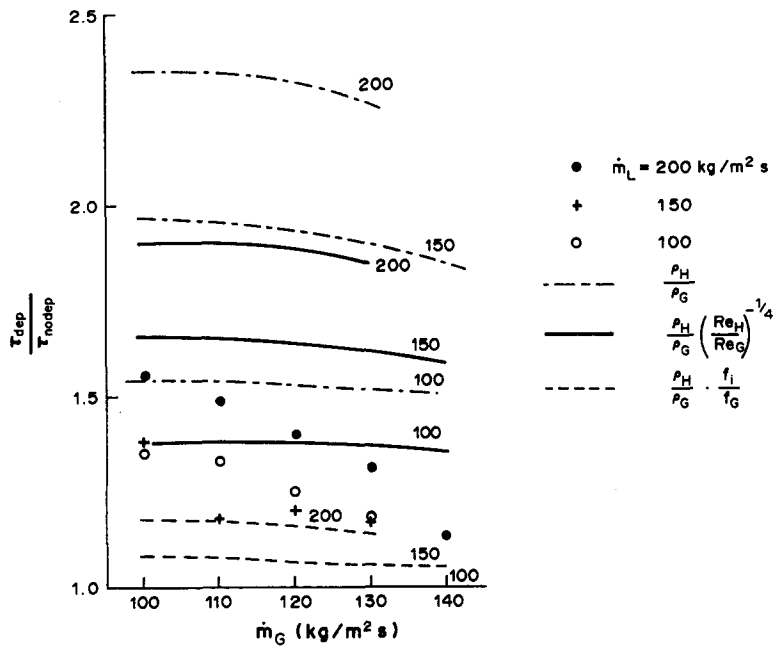

Figure 12. Shear stress enhancement due to droplets.

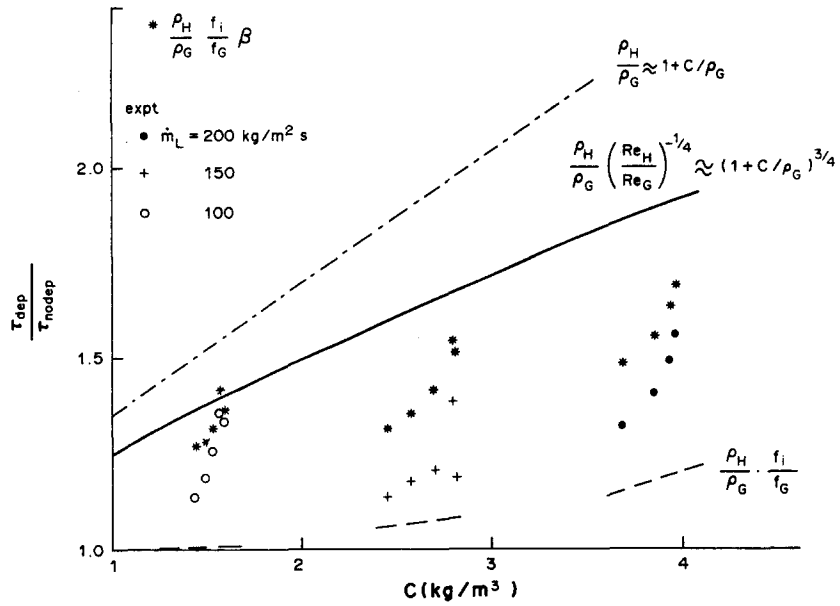

Figure 13. Shear stress enhancement vs droplet concentration.

and f_{gsc} is the smooth pipe friction factor for a Reynolds number Re_H defined by the expression

$$Re_H = \frac{U_G \rho_H d_0}{\mu_G}. \quad [26]$$

Assuming that $\tau_i \approx \tau_0$ for the thin films of the present experiments and that δ is not changed by droplet deposition, and assuming the Blasius relationship for f_{gsc}, equations such as [23] and [24] lead to the expression

$$\frac{\tau_{dep}}{\tau_{nodep}} = \frac{\rho_H}{\rho_G}\left(\frac{Re_H}{Re_G}\right)^{-1/4} = \left(\frac{\rho_H}{\rho_G}\right)^{3/4}. \quad [27]$$

Curves calculated from [27] are also plotted in figures 12 and 13 and though the discrepancy is less than for [22], a considerable overprediction still occurs.

It is clear that the measured shear stress is much lower than predicted from the above commonly used procedures and one must seek an explanation in more recent findings about the influence of droplets on gas core turbulence. Studies reported by Owen & Hewitt (1987) show that the mixing length in the gas core is reduced in the presence of droplets and they introduced a modified friction factor equation to take account of this. This was adapted from the classical Nikuradse equation and had the following form:

$$\sqrt{\frac{2}{f_i}} = \frac{1}{K_{TP}}\ln\left(\frac{R_i}{\epsilon}\right) + A_r - \frac{1.5}{K_{TP}} + \frac{1}{K_{TP}}\left(\frac{2\delta}{R_0}\ln\frac{R_0}{\delta} - \frac{\delta}{R_0}\right), \quad [28]$$

where A_r is the Nikuradse sand roughness parameter, K_{TP} is a two-phase Von Karman constant, R_i and R_0 are the interfacial and wall radii and ϵ is the effective roughness of the liquid film. In unidirectional deposition the film is very thin and, making the additional assumption that it is fully rough (so $A_r = 8.5$), the equation reduces to

$$\sqrt{\frac{2}{f_i}} = \frac{1}{K_{TP}}\left(\ln\frac{R_0}{\epsilon} - 1.5\right) + 8.5. \quad [29]$$

Owen *et al.* gave a correlation for K_{TP} as a function of

$$\frac{\rho_G U_G^2}{\rho_H U_{GC}^2} \simeq \frac{\rho_G}{\rho_H}.$$

Assuming the roughness of the depositing film is the same as the "no-deposition" film, this gives

$$\frac{\tau_{dep}}{\tau_{nodep}} = \frac{f_i}{f_G}\frac{\rho_H}{\rho_G} = \frac{\rho_H}{\rho_G}\left(\frac{K_{TP}}{K_{SP}}\right)^2\left(\frac{\ln\frac{R_0}{\epsilon} - 1.5 + 8.5\,K_{SP}}{\ln\frac{R_0}{\epsilon} - 1.5 + 8.5\,K_{TP}}\right)^2. \quad [30]$$

Calculations from [30] are shown in figure 12. Now, the enhancement of shear stress is *unpredicted* and it is clear that the reduction in mixing length (turbulence) due to the droplets is obviously an important factor. The data are also plotted and compared with [22], [27] and [30] in figure 13 where the parameter plotted is C (the droplet concentration) rather than $\dot{m}_G$. The discrepancy increases with increasing concentration.

Carrying this analogy with homogeneous flow a step further, it will be seen that a closer parallel to the present situation would be that of condensation. There is mass deposition on the interface in both cases, in the form of molecules in condensation and in the form of droplets in the present experiments. As is well-known, the condensation process leads to an enhancement of interfacial shear stress and this enhancement is often calculated from the "equivalent laminar film theory" (e.g. Bird *et al.* 1960). The shear stress is enhanced by a factor β, where β is given by

$$\beta = \frac{F}{\exp(F) - 1} \quad [31]$$

and

$$F = \frac{-2\dot{m}_c}{\rho_G f_{i0}(u_G - u_L)}, \quad [32]$$

where $\dot{m}_c$ is the condensation rate per unit peripheral area, f_{i0} is the interfacial friction factor in the absence of condensation and u_G and u_L are the gas and liquid velocities, respectively. Suppose that, for the unidirectional deposition tests, the deposition rate D can be considered equivalent to $\dot{m}_c$. Assuming that $u_G \gg u_L = U_G$, then [32] becomes

$$F = \frac{-2D}{\rho_G \cdot \frac{\tau_{nodep}}{\frac{1}{2}U_G^2\rho_G} \cdot U_G} = \frac{-U_G D}{\tau_{nodep}} = \frac{-\dot{m}_G D}{\rho_G \tau_{nodep}}. \quad [33]$$

Note that the factor β has a similar form to the enhancement predicted by [21], but has an additional factor $1/[\exp(F) - 1]$ which arises because the shear stress contributions are not simply additive, as assumed in [21]. At high values of D, [31] becomes equivalent to [21].

Values of β can then be determined and are shown in table 3. The final equation for τ_{dep}/τ_{nodep} then becomes

$$\frac{\tau_{dep}}{\tau_{nodep}} = \frac{f_i}{f_G} \cdot \frac{\rho_H}{\rho_G} \cdot \beta. \quad [34]$$

Values calculated from [34] are plotted in figure 13 and it will be seen that, though the values lie a little higher than the measured values, the trends are correctly predicted. Thus, the condensation analogy appears to work rather well. This finding is rather remarkable in that, in the case of condensation, the condensing molecules ultimately join the film at the interface velocity and this is unlikely to be the case with the droplets. In fact, the agreement is well within that which might have been expected from the Owen & Hewitt (1987) analysis. Indeed, there may be deficiencies in this analysis in the representation of the turbulence suppression; recent work by Teixeira & Azzopardi (1989) has suggested that the suppression may be a strong function of drop size and this would need to be accounted for.

4. CONCLUSIONS

The following main conclusions may be drawn from this work:

(1) New measurements have been made of wall shear stress in equilibrium annular air–water flow covering a wide range of phase flowrates. The results for mean

wall shear stress are shown to be consistent with the measurements of pressure drop along the channel and, at high liquid mass fluxes, show the characteristic maximum and minimum as a function of gas mass flux, as had first been observed for the pressure gradient data.

(2) Analysis of the fluctuations in wall shear stress in annular flow shows the existence of a peak frequency corresponding to the passage frequency of disturbance waves along the interface. This peak frequency increases with gas mass flux but becomes less distinct at higher gas mass fluxes. The influence of liquid mass flux on peak frequency is relatively small.

(3) A series of experiments were conducted on shear stress in the unidirectional droplet deposition region following film removal in a fully-developed annular flow. Measurements of pressure gradient and deposition rate were also made in this region. Comparing the pressure gradient with that measured for the same film flowrate in the absence of droplets, it was found that the pressure gradient could be reduced. This was shown to be consistent with the measured shear stress and deposition rate data.

(4) The wall shear stress in the unidirectional deposition region (τ_{dep}) was compared with that for a (subcritical) film at the same mass flowrate but without the presence of droplets (τ_{nodep}). Commonly used assumptions about the enhancement were shown to grossly overpredict the enhancement of shear stress by droplet deposition.

(5) The data for τ_{dep}/τ_{nodep} were compared with a new theory by Owen & Hewitt (1987) which takes account of the reduction in mixing length (turbulence) in the gas core resulting from the presence of the droplets. This theory gave much closer agreement but the values of τ_{dep}/τ_{nodep} were now underpredicted. The agreement could be improved by allowing for enhancement of shear using the "equivalent laminar film" model in a manner analogous to condensation.

Acknowledgement—The work described in this report was carried out as part of the Underlying Research Programme of the UKAEA.

REFERENCES

AZZOPARDI, B . J., FRYER, P. J. & FREEMAN, G. 1979 The frequency of disturbance waves in annular two-phase flow. UKAEA Report AERE-R9347.

BELLHOUSE, B. J. & SCHULTZ, D. L. 1966 Determination of mean and dynamic skin friction, separation and transition in low-speed flow with a thin-film heated element. *J. Fluid Mech.* **24,** 379–400.

BIRD, R. B., STEWART, W. E. & LIGHTFOOT, E. N. 1960 *Transport Phenomena.* Wiley, New York.

COGNET, G., LEBOUCHE, M. & SOUHAR, M. 1984 Wall shear stress measurements by electrochemical probe for gas–liquid two-phase flow in vertical duct. *AIChE Jl* **30,** 338–341.

COUSINS, L. B. & HEWITT, G. F. 1968 Liquid phase mass transfer in annular two-phase flow: droplet deposition and liquid entrainment. UKAEA Report AERE-R5657.

CRAVAROLO, L., GIORGINI, A., HASSID, A. & PEDROCCHI, E. 1964. A device for the measurement of shear stress on the wall of a conduit—its application in the mean density determination in two-phase flow shear stress data in two-phase adiabatic vertical flow. CISE (Milan) Report No. R-82.

GOVAN, A. H., HEWITT, G. F., OWEN, D. G. & BOTT, T. R. 1988 An improved CHF modelling code. Presented at *2nd U.K. Natn. Heat Transfer Conf.*, Strathclyde Univ., Glasgow.

HEWITT, G. F. 1982 Prediction of pressure drop in annular flow by phenomenological modelling. In *Handbook of Multiphase Systems*, Chap. 2.2.4 (Edited by HETSRONI, G.). McGraw-Hill, New York.

HEWITT, G. F. & HALL-TAYLOR, N. S. 1970 *Annular Two-phase Flow.* Pergamon Press, Oxford.

KIRILLOV, P. L., SMOGALEV, I. P., SUVOROV, M. YA, SHUMSKY, R. V. & STEIN, YU. 1978 Investigation of steam–water flow characteristics at high pressures. *Proc. 6th Int. Heat Transfer Conf., Toronto* **1,** 315–320.

KUTATELADZE, S. S., BURDUKOV, A. P., NAKORYAKOV, V. YE. & KUZMIN, V. Z. 1969 Application of an electrochemical method for the measurement of shear stress in two-phase flow. *Heat Transfer Sov. Res.* **1,** 69–73.

MARTIN, C. J. 1983 Annular two-phase flow. Ph.D. Thesis, Oxford Univ.

OWEN, D. G. 1986 An experimental and theoretical analysis of equilibrium annular flow. Ph.D. Thesis, Birmingham Univ.

OWEN, D. G. & HEWITT, G. F. 1987 An improved annular two-phase flow model. Presented at *3rd Int. Conf. on Multiphase Flow*, The Hague.

OWEN, D. G., HEWITT, G. F. & BOTT, T. R. 1985 Equilibrium annular flows at high mass fluxes; data and interpretation. (Presented at *Int. Symp. on Two-phase Annular and Dispersed Flows*, Univ. of Pisa, June 1984.) *PhysicoChem. Hydrodynam.* **6,** 115–131.

SEKOGOUCHI, K., TAKEISHI, M. & ISHIMKATSU, T. A. 1985 Interfacial structure in vertical upward annular flow. (Presented at *Int. Symp. on Two-phase Annular and Dispersed Flows*, Univ. of Pisa, June 1984.) *PhysicoChem. Hydronam.* **6,** 239–255.

SHIRALKAR, B. S. 1970 Two-phase flow and heat transfer in multi-rod geometries: a study of the liquid film in adiabatic air–water flow with and without obstacles. General Electric Report GEAP-10248.

TEIXEIRA, J. C. F. & AZZOPARDI, B. J. 1989 Harwell data. To be published.

WALLIS, G. B. 1979 Annular two-phase flow, Part I: a simple theory; Part II: additional effects. *J. basic Engng* **92,** 59–82.

WHALLEY, P. B. & HEWITT, G. F. 1978 The correlation of liquid entrainment fraction and entrainment rate in annular two-phase flow. UKAEA Report AERE-R9187.

WHALLEY, P. B. & MCQUILLAN, K. W. 1985 The development and use of a directional wall shear stress probe. Presented at *2nd Int. Conf. on Multiphase Flow*, London, Paper G2.

ZABARAS, G. 1985 Studies in vertical annular gas–liquid flow. Ph.D. Thesis, Houston, Tex.